MDPI

Article

New Approach for Sulfidation Process in Packed Bed with Hi-Fuel A310 Sorbent—Thermodynamical Studies

Clarisse Lorreyte [1,*], Barbara Malinowska [1], Vincent Butin [1], Nathalie Ruscassier [1], Joel Casalinho [1] and Patrick Perré [1,2]

[1] Université Paris-Saclay, CentraleSupélec, Laboratoire Génie des Procédés et Matériaux (LGPM), 91 190 Gif-sur-Yvette, France; barbara.malinowska@centralesupelec.fr (B.M.); vincent.butin@centralesupelec.fr (V.B.); nathalie.ruscassier@centralesupelec.fr (N.R.); joel.casalinho@centralesupelec.fr (J.C.); patrick.perre@centralesupelec.fr (P.P.)

[2] Université Paris-Saclay, CentraleSupélec, Laboratoire Génie des Procédés et Matériaux (LGPM), Centre Européen de Biotechnologie et de Bioéconomie (CEBB), 51 110 Pomacle, France

* Correspondence: clarisse.lorreyte@centralesupelec.fr

Abstract: This paper presents tests related to the reactivity of commercial Hi-Fuel sorbent toward H_2S (H_2S/N_2 mixture) in a packed bed at 300 °C. The sorbent used for breakthrough test was characterized before and after test by ESEM-EDX, FTIR-ATR, Raman, and elemental analyses. Testing reveals that the commercial sorbent contains two compounds reacting with H_2S: ZnO and $ZnCO_3$. According to thermodynamical studies, the reactivity of $ZnCO_3$ at 300 °C is privileged ($K_R = 9.5 \times 10^8$) than ZnO ($K_R = 6.6 \times 10^6$). In addition, the reaction of H_2S with $ZnCO_3$ induces a volume decrease, which promotes the movement of gas through the newly formed layer. The properties of this sorbent thus hold a good potential for the desulfurization process of gases polluted with H_2S. We observed that the maximum sulfidation rate was reached on the surface of the sorbent and showed a maximum conversion of 27%.

Keywords: desulfurization; zinc oxide; zinc carbonate; thermodynamic studies; biomass

1. Introduction

The transformation of lignocellulosic feedstock and the recycling of carbonaceous is essential for reducing reliance on fossil fuels in the energy and transport sectors. The syngas obtained by the thermochemical conversion (gasification process) of biomass consists mainly of H_2, CO, CO_2, and some quantity of CH_4 (depending on the type of biomass and operations conditions). Unfortunately, impurities such as tars, particulate matter, NH_3, H_2S, HCl, and SO_2, all produced during the gasification, remain in the resulting syngas [1]. These pollutants cause severe problems in downstream applications. For example, H_2S is a corrosive gas at the industrial level and a poison for metal sorbents used in the gas industry [2,3]. H_2S also presents acute toxicity and is responsible for serious environmental damage.

In response to the issues caused by fossil fuel reliance, hydrogen fuel cells have emerged as a high potential technology for mobility, offering significant energy efficiency and decarbonization benefits to various industries, including automotive and heavy transport. The production of hydrogen by thermochemical conversion of biomass is a renewable and potentially competitive alternative to other sources of hydrogen, such as hydrocarbon reforming or water electrolysis.

However, unlike petrol cars, hydrogen fuel cell vehicles are very sensitive to fuel purity. According to the 2019 standard [4], the current level of hydrogen purity required for this application admits 4 ppbv H_2S [4]. But according to recent data, in the Toyota Mirai, even 4 ppb of hydrogen sulfide can destroy the fuel cell [5].

This deep desulfurization of a gas can be achieved using the capture of H_2S with metal oxides. Oxides such as ZnO, CuO, or NiO are used on an industrial scale for this purpose, as they can react with H_2S to form the corresponding metal sulfide.

Indeed, from many studies, ZnO is considered very effective in the removal of H_2S [6–12] and appears to be one of the best candidates as metal oxide for syngas desulfurization [13] (Equation (1)).

$$ZnO \text{ (s)} + H_2S \text{ (g)} \rightarrow ZnS \text{ (s)} + H_2O\text{(g)} \tag{1}$$
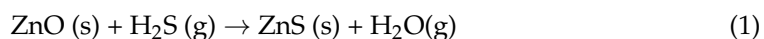
Another advantage of ZnO, is the reversibility of the reaction ZnO to ZnS and so the option to recycle the sorbent after reaction.

Two of the most commonly used models to describe the kinetics sulfidation of zinc oxide are the shrinking core model [6,14,15] and the hollow core-shell model [8,10,16]. In both models, the selected equations result in a reaction at the surface of the absorbent while the core of the reactant remains most of the time unconverted.

Other studies have previously demonstrated the existence of limitations due to solid state diffusion, both in the ZnS layer formed during the reaction and at the ZnO/ZnS interface [8,17]. The ZnO sorbent properties are mainly dependent on the preparation methods (precipitation mode, pH, type of reactants), which influence the final ZnO morphology.

These studies show that ZnO with very developed surface area can be prepared from basic zinc carbonate $Zn_3CO_3(OH)_4$, via previous chemical reaction, followed by its thermal decomposition [18], (Equation (2)).

$$Zn_3CO_3(OH)_4 \text{ (s)} \rightarrow ZnO \text{ (s)} + CO_2 \text{ (g)} + 2H_2O \text{ (g)} \tag{2}$$
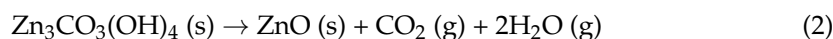
Another way of producing ZnO is by thermal reaction of hydrozincite $Zn_5(CO_3)_2(OH)_6$. This compound heated at 500 °C decomposes into ZnO [19], (Equation (3)).

$$Zn_5(CO_3)_2(OH)_6 \text{ (s)} \rightarrow 5ZnO \text{ (s)} + 2CO_2 \text{ (g)} + 3H_2O \text{ (g)} \tag{3}$$

Kowalik et al. [20] demonstrated the essential changes of ZnO morphology through CO_2 saturation of the aqueous suspension of the raw ZnO. During the subsequent thermal decomposition, a porous structure is created together with a drastic increase of the specific surface area. These changes lead to the conversion of "common" zinc oxide into active zinc oxide.

Balichard et al. [21] performed the study of pure $ZnCO_3$ reactivity towards H_2S (Equation (4)).

$$ZnCO_3 \text{ (s)} + H_2S \text{ (g)} \rightarrow ZnS \text{ (s)} + CO_2 \text{ (g)} + H_2O \text{ (g)} \tag{4}$$

They showed that the sulfidation was complete for $ZnCO_3$ in the range 140–180 °C. Furthermore, the process is not controlled by diffusion, as in ZnO's case, because the generated ZnS layer is discontinuous. As a result, the gas desulfurization capacity by $ZnCO_3$ is higher than ZnO.

In summary, the preparation method of commercial sorbents is often unknown to the purchaser and must be tested before industrial application.

This work is part of a project devoted to the production of hydrogen from biomass. Despite the interest of this source of hydrogen, the decontamination of the syngas issued from biomass is crucial. For this reason, our study focuses on the desulfurization process using the commercial sorbent Hi-Fuel A310. This sorbent was chosen, among others, for its high content of ZnO and its spherical shape, convenient and appropriate for the use as a packed bed. Also, the price of this sorbent was interesting since it was one of the less expensive. Since in our study, the H_2S concentration in studied gas was low and since the price of the sorbent was low, we planned the use of this sorbent as sacrificial. So, even though the used ZnO sorbent can be recycled, we did not study this aspect.

The sorbent is analyzed before and after the sulfidation test in a packed sorbent bed. Testing is stopped after the H_2S breakthrough. At the end of the experiment, all

analyses describe the sorbent state along the bed height. To better understand the obtained results, we performed thermodynamical calculations which demonstrate that the chemical composition of sorbent plays an important role in the efficiency of gas desulfurization. Unlike many works in which ZnO or $ZnCO_3$ are used separately as sorbents, our work proposes a novel approach by showing that a sorbent composed of both ZnO and $ZnCO_3$ can also be an effective sorbent for H_2S removal.

2. Materials and Methods

2.1. Materials

The sorbent employed in this study is Hi-Fuel A310, was supplied by Alfa Aesar and manufactured by Johnson Matthey. According to the manufacturer, it contains 92% of ZnO supported on 8% of calcium aluminate. The size of the spherical particles ranges from 2.8 to 4.75 mm, and their bulk density is 820 kg/m^3. Our reference ZnS was manufactured by Alfa Aesar and had a purity of 99.99%. $ZnCO_3$ was produced by MP Biomedicals, LLC. All gases used in the experiments are purchased from Air Liquide: the nitrogen certified ALPHAGAZ^{TM} 2 ($N_2 \geq 99.9999\%$) and the mixture of H_2S (1004 ppmv $\pm$ 30 Mol-ppm) in nitrogen quality ALPHAGAZ^{TM} 1 ($N_2 \geq 99.999\%$).

2.2. Experimental Setup

An experimental setup was developed to study the sulfidation reaction at the packed bed scale (Figure 1). The reactor consists of a cylindrical quartz tube, 440 mm high, with an interior diameter of 30 mm. The sorbent (bed height 0.8 cm) loaded in the reactor chamber was maintained by a layer of glass beads.

(**a**)   (**b**)
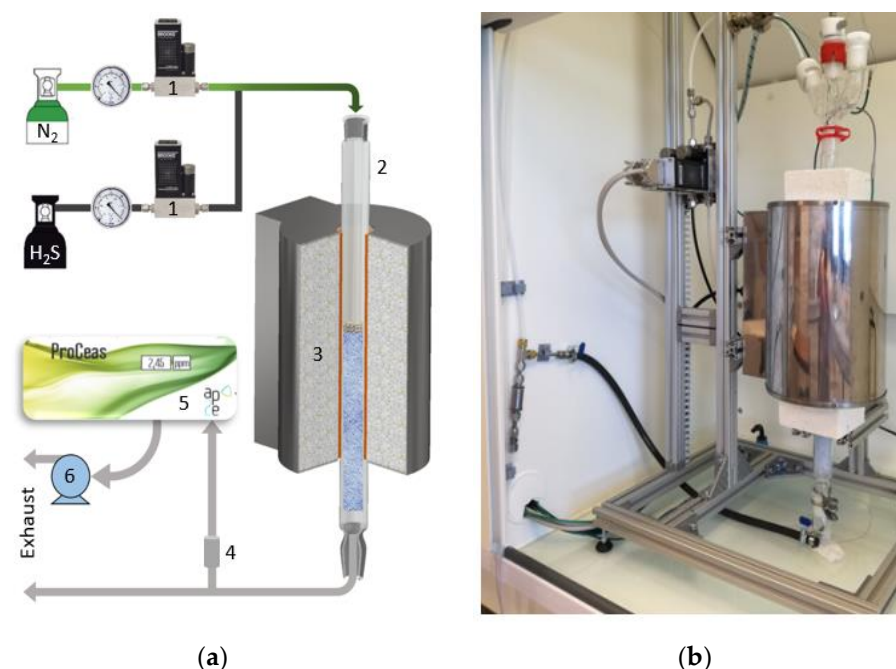
Figure 1. (**a**) Schematic view; (**b**) and picture of the experimental setup used for the sulfidation tests. 1—mass flow meter, Brooks Instrument; 2—glass reactor with an internal diameter of 3 cm; 3—tube furnace; 4—sampling nozzle providing a flow rate of about 3 L/h through the AP2E analyzer; 5—AP2E analyzer; 6—AP2E analyzer pump.

This reactor was introduced vertically in a tubular furnace (MTF 12/38A, Carbolite furnaces, Sheffield, UK). At the beginning of the experiment, pure nitrogen at room temperature was passed through the reactor at 60 NmL/min for 24 h to remove oxygen. Then the sorbent was heated to 300 °C under the same flow rate of pure nitrogen for 6 h. Finally, the reactive gas (mixture of H_2S and N_2) passed through the reactor at the same flow rate. This

gave a Gas Hourly Space Velocity (GHSV) of 637 h^{-1}. During this purification step, the initial mixture of 1000 ppmv H_2S in N_2 was diluted upstream with pure N_2 to reach the desired concentration of H_2S using two mass flow controllers (SLA 5850S, Brooks Instrument, Hatfield, PA, USA). A laser infrared spectrometer adapted for low level detection of H_2S in gas measured the outlet H_2S concentration. The infrared source was a non-pulsed laser. The patented Optical Feedback Cavity Enhanced Absorption Spectroscopy (OFCEAS) technology and infrared laser technology were applied in a spectrometer (ProCeas® H_2S, AP2E, Aix en Provence, France). It contained a gas cell equipped with highly high reflectivity mirrors enabling pathlength from 1000 to 10,000 m in a measurement vessel featuring an internal volume of only 15 mL. This gas sampling was known as Enhanced Cavity. This analyzer can also detect carbon dioxide and water vapor. At the end of the sulfidation test, we used pure nitrogen again during the cooldown.

2.3. Analytical Methods

We performed analyses for fresh and converted sorbents. The converted sorbents were from thermogravimetric analysis and packed bed sulfidation test. The original size of particles was taken for: thermogravimetric analysis TGA-DSC, specific surface area determination (BET), and scanning electron microscopy (ESEM). We prepared powdered samples for infrared spectroscopy (FTIR-ATR), Raman spectroscopy, and elemental analysis. These powders were obtained by using an agate mortar. In the case of a sample from TGA analysis, one single particle was powdered. In other cases, (fresh, thermal treated, or sulfided sorbent), the powder was obtained from 4 particles. All samples were stored under vacuum conditions until further analysis. Given that the color of sulfided particles is not homogenous, the mixed yellow and dark grey particles were milled.

2.3.1. Thermogravimetric Analysis

The TGA apparatus was a thermogravimetric analyzer (STA 449 F1 Jupiter, NETZSCH) with a weighing sensitivity of 0.025 μg and a balance drift lower than 2 μg/h. We used the TGA-DCS sample carrier to measure mass loss and heat flux simultaneously. The initial mass of the sample was ca. 20 mg (single particle). The experiments ran under a 50 NmL/min nitrogen flow and a 20 NmL/min protective gas flow. We started the test by heating the sample to 30 °C for a 30-min plateau, followed by a heating phase at 10 K/min to 400 °C and a 30-min plateau at this final temperature. All tests were blank corrected with the same crucible as for the experiment.

2.3.2. Specific Surface Area Determination

The BET device (3Flex, Micromeritics, Norcross, USA) measures surface area, pore size, and pore volume. The samples were maintained at 80 °C for 24 h for the degassing phase. Following these 24 h, the BET device determined the surface area and pore distribution at the boiling temperature of liquid nitrogen (−195.8 °C). Once the liquid nitrogen reached the boiling temperature, we used an interval of 5 s to allow equilibrium at each measurement point. We then applied the Brunauer-Emmett-Teller (BET) model for the specific surface area determination and BJH (Barret-Joyner-Halenda) transformation for mesopores characteristic [22–24].

2.3.3. Environmental Scanning Electron Microscopy (ESEM)

The samples were observed in an Environmental Scanning Electron Microscope (ESEM Quanta 200, FEI) used in low vacuum. We determined the chemical composition of the particles by quantitative Energy Dispersive X-ray Spectroscopy (EDX EDAX, Software-Genesis 5.3) in the ESEM. Each sample (particle) was cut into two half spheres. One was placed on the sample holder with the cross section upwards. We performed four EDX analyses along three different radii (center, 1/3 of the radius, 2/3 of the radius, and the surface). An EDX mapping of the cross section of the particle was performed. Two samples were observed and analyzed for each layer of the bed.

2.3.4. Fourier Transform Infrared Spectroscopy—Attenuated Total Reflectance (FTIR—ATR)

We performed the analyses with Spectrum Two (Perkin Elmer, Inc., Beaconsfield, UK) equipped with a ZnSe crystal with an incidence angle of 45° et 25 reflections. The background spectra were recorded in the air. The conditions of spectra acquisitions for powdered samples were the following: 16 scans in the range 400–4000 cm^{-1} with 4 cm^{-1} resolution.

2.3.5. Raman Spectroscopic Study

The Raman spectra of powdered samples were examined using a confocal Raman microscope (Alpha 300R+, WITec GmbH, Ulm, Germany). Each spectrum was collected with a 532 nm laser at 10 mW and an integration time of 6 s. The average optical resolution was 4 cm^{-1}. Ten accumulations were realized for each sample with a spectral range of 90–1250 cm^{-1}.

### 2.3.6. Elemental Analysis (C, H, N, S)

The elemental composition of samples was carried out with an elemental analyzer (FLASH 2000, Thermo Fisher Scientific, Courtaboeuf, France). We used 1–2 mg of powder. Furthermore, each CHNS analysis was performed by adding 1 mg of V_2O_5 into each sample. The addition of V_2O_5 is usually applied for the complete combustion of sample containing a sulfur. Each measurement was done in duplicate.

3. Results and Discussion

3.1. Breakthrough Curve

The total duration of the experiment was 22 days: first, 7 days with 100 ppm of H_2S at the inlet of reactor followed by 167 ppm of H_2S for 15 days. We expected the breakthrough with 100 ppm but since we did not obtain it after 7 days, we decided to increase the input concentration of H_2S to167 ppm.

Finally, we observed the breakthrough after 13 days of experiment, thus 6 days after increasing the H_2S inlet concentration (Figure 2). Until the observation of breakthrough, H_2S was captured by the packed bed of the sorbent.
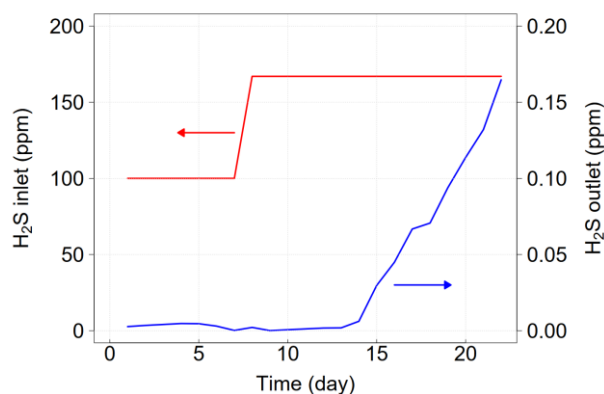
Figure 2. Breakthrough curve for 0.8 cm height Hi-Fuel sorbent at 300 °C with the injection of 100 ppm H_2S for 7 days followed by 167 ppm H_2S for 15 days. Gas flow of mixture H_2S/N_2—60 NmL/min (GHSV = 637 h^{-1}).

We can observe a color change between converted sorbent (from sulfidation test) and fresh sorbent (Figure 3). The fresh balls of sorbent had a uniform light grey color (Figure 3a). After sulfidation, a graduation of the sorbent color was observed from the top to the bottom of the bed: dark grey at the top to yellow at the bottom (Figure 3b). Nevertheless, sometimes, dark grey and yellow balls were mixed in the same layer, probably due to preferential flow pathways. In addition, we noted that the upper part of many balls exposed to the gas flow containing H_2S arriving from the top of reactor, is rather dark grey than yellow. It should

be noted that, the characteristic color of ZnS is yellow. To analyze the spatial evolution of sulfidation in the packed bed, we divided the packed bed into three layers.
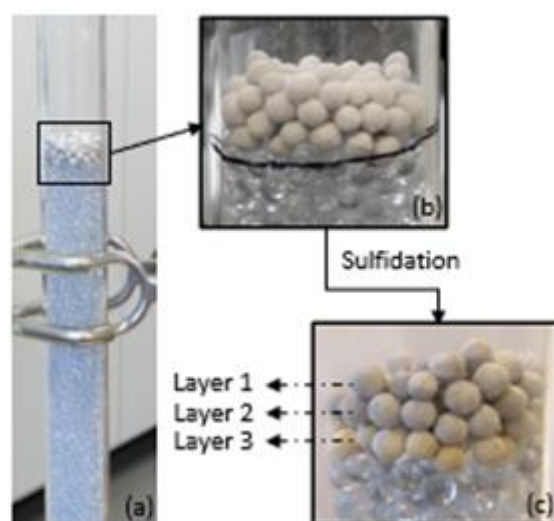
Figure 3. Photographs of the sorbent; (**a**) in the reactor supported by glass beads before sulfidation; (**b**) close-up view of the sorbent; (**c**) after sulfidation with the three layers selected along the packed bed height.

3.2. Characterization of Sorbent before and after Sulfidation

The surface area and the porosity of sorbents impact the efficiency of sulfidation. The results of these analyses for the Hi-Fuel A310 sorbent used in our test are reported in Table 1.

Table 1. Comparison of specific surface area (BET) and characteristic of the pore structure of the fresh sorbent, thermally treated at 300 °C for 6 h and the converted sorbent from packed bed scale.

Sorbent	Surface Area (m²/g)	Average Pore Diameter(Å)	Single Point Adsorption Total Pore Volume of Pores Less than 403.122 Å Diameter at p/p° = 0.95 (cm³/g)	Pore Volume of Mesopores by BJH, Diameter between 17 and 3000 Å (cm³/g)
Fresh	52.6	117.2	0.154	0.215
Thermally treated at 300 °C for 6 h	51.9	122.7	0.162	0.268
Converted sorbent from packed bed scale at 300 °C				
Layer 1	44.6	112.7	0.132	0.206
Layer 2	50.5	120.1	0.152	0.200
Layer 3	51.6	117.7	0.152	0.214

Results (Table 1) show that the thermal treatment at 300 °C induced a slight decrease of the specific surface (1.3%). The thermal treatment increases the average pore diameter and also increases the mesopores volume by about 25%.

The outer layer of the sorbent was less dense than the sorbent core-shell (Figure 4b). The thermal treatment might enhance the porosity of this layer covering the core-shell. Finally, the observed changes are beneficial for the subsequent step, namely sulfidation, because the well-developed pore system facilitates the diffusion of H_2S inside the sorbent and the outwards displacement of released water according to the Equation (1).

The increase of the mesopore volume is very interesting knowing that the internal structure of fresh Hi-Fuel A310 sorbent is not homogenous (Figure 4).

The sulfidation of ZnO involved another unavoidable structural change of the sorbent. Since the sulfide ion is much larger than the oxide ion, the ZnS crystalline lattice volume was expanded compared to ZnO crystalline lattice volume by a factor of 1.60 [8].

(**a**)　　　　　　　　　　　　　　　(**b**)　　　　　　　　　　　　　　　(**c**)
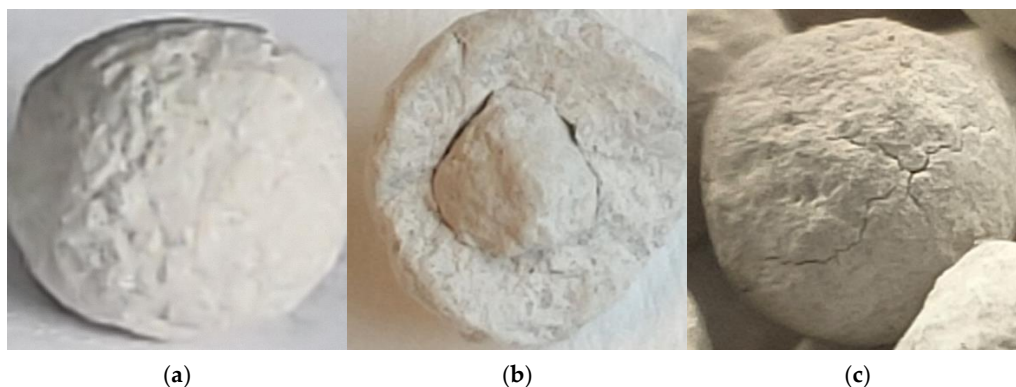
Figure 4. (**a**,**b**) Pictures of fresh Hi-Fuel A310 sorbent; (**c**) converted sorbent.

For this reason, the sorbent pore network narrowed as the sulfurization progressed and was eventually wholly blocked to gas transfer. The crystalline structure's swelling might also induce cracking of the outer layer, as depicted in Figure 4c.

The sulfidation process always induces a reduction of the surface area. In our study, the surface area of the first layer decreased by 15.3% and the diameter of pores was also reduced. The surface areas of the second and third layers are respectively reduced by 4.0% and 1.8%.

The efficiency of sulfidation and induced sorbent changes depends on several factors, e.g., the size of sorbent particles, the specific surface area, the process temperature... When the sorbent has a size of nanoparticles, the in-depth access of H_2S inside the sorbent is more accessible, and higher sulfidation ratios can also be obtained [7].

Representative results of ESEM/EDX studies on the dark greys particles of converted sorbent belonging to three layers are depicted in Figure 5.
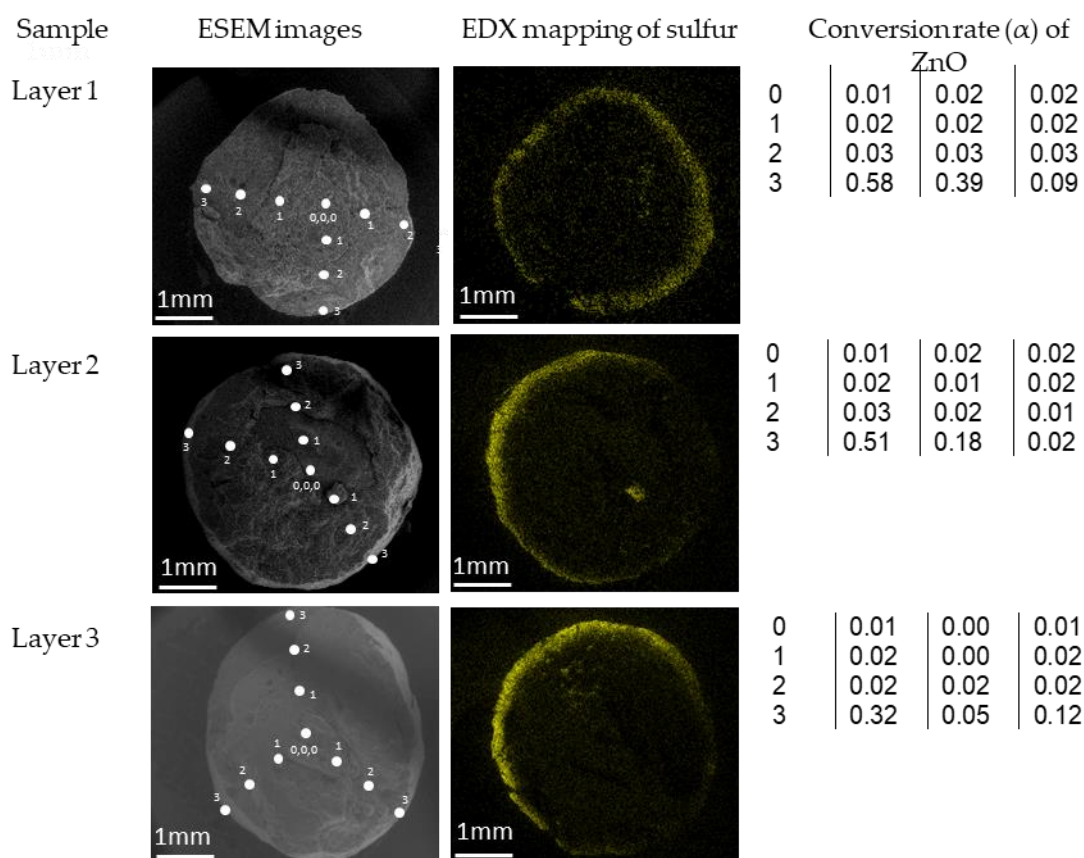
Sample	ESEM images	EDX mapping of sulfur	Conversion rate (α) of ZnO		
Layer 1			0 0.03	0.04	0.01
			1 0.05	0.06	0.03
			2 0.79	0.33	0.04
			3 0.82	0.88	0.78
Layer 2			0 0.02	0.02	0.02
			1 0.02	0.02	0.02
			2 0.56	0.03	0.02
			3 0.75	0.58	0.32
Layer 3			0 0.03	0.02	0.02
			1 0.03	0.03	0.02
			2 0.15	0.29	0.03
			3 0.92	0.71	0.38

Figure 5. ESEM pictures and elemental mapping obtained for dark grey particles of transformed sorbent from packed bed scale process at 300 °C.

According to the elemental mapping obtained for the converted sorbent, ZnO sulfidation occurred throughout the bed height. But the distribution of sulfur inside the sorbent particles was not homogenous. The concentration of sulfur was the highest on the sorbent's surface, and we observed a gradient in the radial direction from the center to the surface.

In addition, the EDX quantitative analysis also enabled the determination of ZnO's conversion rate (α) into ZnS. The conversion rate is defined by the ratio of sulfur atomic percentage to zinc atomic percentage. High conversion ratios of ZnO into ZnS were manifest in the particle's external layers, while the core mainly remained unconverted (as already observed by many authors [8,16,25]).

In the case of yellow beads, the distribution of sulfur was mainly in the external layers but with a lower level of sulfidation compared to dark grey balls (Figure 6). Thus, when ZnS is only formed at the sorbent surface, and observed, under exterior lighting, it confers its characteristic yellow color on the sorbent. On the contrary, when ZnS is formed in the inferior layers of sorbent, the exterior light cannot go through the depth of the sorbent and so the yellow color cannot be observed.

Sample	ESEM images	EDX mapping of sulfur	Conversion rate (α) of ZnO			
Layer 1			0	0.01	0.02	0.02
			1	0.02	0.02	0.02
			2	0.03	0.03	0.03
			3	0.58	0.39	0.09
Layer 2			0	0.01	0.02	0.02
			1	0.02	0.01	0.02
			2	0.03	0.02	0.01
			3	0.51	0.18	0.02
Layer 3			0	0.01	0.00	0.01
			1	0.02	0.00	0.02
			2	0.02	0.02	0.02
			3	0.32	0.05	0.12

Figure 6. ESEM pictures and elemental mapping obtained for yellow particles of transformed sorbent from packed bed scale process at 300 °C.

The elemental analysis of powdered sorbent samples confirmed the sulfidation of ZnO by H_2S (Table 2).

According to these results, the fresh sorbent contains hydrogen, carbon, and oxygen.

Two first elements (hydrogen and carbon) are not part of the compounds listed in the manufacturer certificate. The results also show that the sorbent thermally treated before sulfidation has partially lost these elements. Furthermore, the average conversion rate (α) of ZnO to ZnS for each layer in packed bed was calculated. In this case the value of α corresponds to the ratio of number of sulfur moles to the number of ZnO moles.

Table 2. Elemental analysis of fresh and thermally treated (300 °C for 6 h) sorbent compared with converted sorbent from packed bed scale process.

Sorbent	Carbon [%]	Hydrogen [%]	Sulfur [%]	Oxygen [%]	Mean Conversion Rate (α) of ZnO into ZnS Calculated for Each Layer of Converted Sorbent
Fresh	1.18	0.48	0	19.16	-
Thermally treated at 300 °C for 6 h	0.85	0.21	0	12.58	-
Converted sorbent from packed bed scale at 300 °C					
Layer 1	0.65	0.18	10.13	12.54	0.27
Layer 2	0.76	0.18	3.99	13.58	0.11
Layer 3	0.75	0.18	3.06	10.43	0.08

We note that the highest mean sulfidation ratio ($\alpha = 0.27$) observed in the 1st layer is concomitant with the highest loss of carbon. The 2nd and 3rd layers show lower sulfidation ratios: 0.11 and 0.08. At the same time, the hydrogen concentration in the three layers decreases slightly compared to the level measured in the thermally treated sorbent. Its final level seems independent of the sulfidation rate.

In many studies, the synthesis of zinc oxide is achieved via precipitation and subsequent thermal treatment of various forms of carbonates: anhydrous, hydrated, and hydroxy or basic carbonates [18,20,26]. For this reason, we performed FTIR-ATR analyses of our samples and compared them with pure $ZnCO_3$ and ZnO (Figure 7).
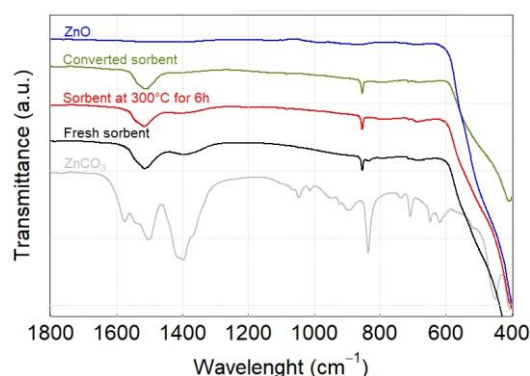

Figure 7. Fourier Transform Infrared—Attenuated Total Reflectance (FTIR-ATR) spectra of the fresh, thermally treated at 300 °C for 6 h and converted Hi-Fuel A310 sorbents from packed bed scale process compared with pure compounds: ZnO and $ZnCO_3$.

Figure 7 shows the strong vibration bands characteristics of carbonate group: at 854 cm^{-1} (mode ν_2 of carbonate) and at 1385 cm^{-1} and 1514 cm^{-1} (mode ν_3 of carbonate) [26,27]. Depending on the size of $ZnCO_3$ crystallite, the carbonate group can be observed between 836 and 865 cm^{-1}. Since the crystallite size of the sorbent and $ZnCO_3$ pure powder might be different, it explains the slight difference of the position observed for mode ν_2 of carbonate band in two spectra. The band at 400 cm^{-1} corresponding to Zn-O lattice mode [28,29] confirms the presence of ZnO. The strong and broad band (region from 2950 to 3670 cm^{-1}, not shown here) centered at 3365 cm^{-1} and characteristic of water was observed in the FTIR-ATR spectra.

The comparison of the spectra confirmed the presence of two chemical forms of zinc in the fresh sorbent: ZnO, and $ZnCO_3$. The TGA/DSC analysis of fresh sorbent, carried out in the range from 25 °C to 400 °C, provided supplementary information on the modification of sorbent composition during the thermal treatment (Figure 8).
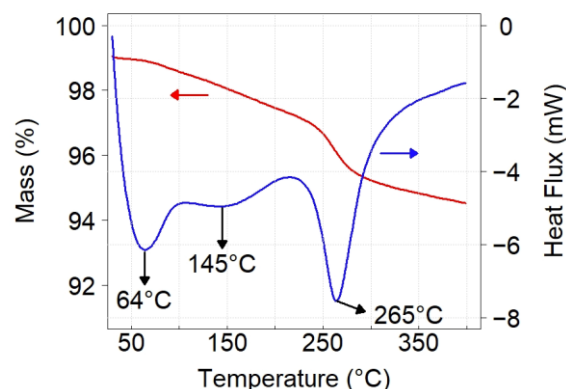
Figure 8. Thermogravimetric Analysis/Differential Scanning Calorimetry (TGA/DSC) of the fresh sorbent Hi-Fuel. (m_0 = 36.62 mg).

The weight loss exhibits three phases. The first one is slow in the temperature range from ambient to about 240 °C, the second one is faster over a short temperature range (240 °C to 270 °C), and the third one is slower and linear decrease up to the remaining temperature range. Three endothermic peaks follow this evolution: at 64 °C, 145 °C, and 265 °C. The two first peaks correspond respectively to removing adsorbed water and crystallization water.

The third endothermic peak, occurring between 220 °C and 300 °C (max at 265 °C), is attributed to the decomposition of zinc carbonate into zinc oxide according to the following equation [18,19,30,31]:

$$ZnCO_3 \text{ (s)} \rightarrow ZnO \text{ (s)} + CO_2 \text{ (g)} \tag{5}$$
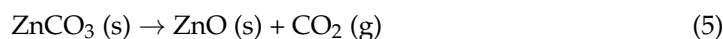
Based on the results from elemental analysis, FTIR-ATR, and TGA/DSC, we concluded that the thermal treatment at 300 °C for 6 h induces the partial decomposition of $ZnCO_3$ and partial removal of water. The carbon released as CO_2 was equal to 1.2% weight loss of the sorbent.

The part of $ZnCO_3$ remaining in this sorbent before sulfidation can be estimated based on elemental analysis. It represented about 8.9 *w/w* %. Following this set of results, the sorbent at the beginning of the sulfidation process contained two forms of zinc compounds, ZnO and $ZnCO_3$, with respective proportions of 89.6 and 8.9%.

We compared the Raman spectrum of the sulfided sorbent with fresh sorbent and pure compounds (Figure 9).
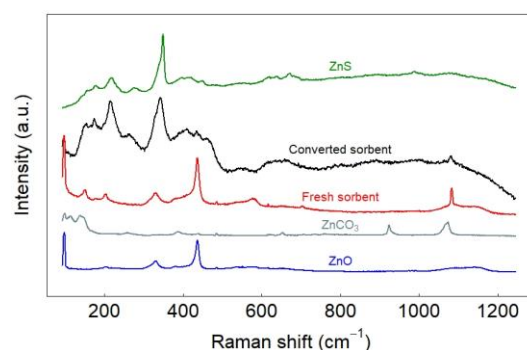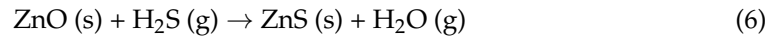

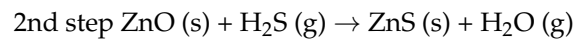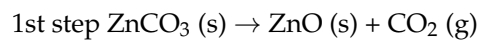**Figure 9.** Raman spectra of the fresh and converted sorbents Hi-Fuel compared with pure compounds: ZnO, $ZnCO_3$, and ZnS.

The Raman bands of converted sorbent indicate the presence of ZnS in the large band ranges from 125 cm^{-1} to 520 cm^{-1} with the strong peak at 345 cm^{-1} and from 590 cm^{-1} to 720 cm^{-1} [32–34] with the signal of low intensity observed. These bands are characteristic of the sphalerite structure for ZnS [34]. According to the thermodynamic data, only sphalerite form should be expected under our operating conditions [35–37].

The characteristic bands of ZnO are evident in the spectra of fresh sorbents: at 98 cm^{-1}, 332 cm^{-1}, and 435 cm^{-1} [38]. In the converted sorbent, these bands are much lower but still present.

Similarly, the characteristic band at 1081 cm^{-1}, ascribed to the symmetric stretching mode of $CO_3{}^{2-}$ (ν_1) from $ZnCO_3$ [19,39], is strong in the fresh sorbent and weaker in the converted sorbent. This band confirms the presence of zinc carbonate and its decreasing concentration during sulfidation. Based on these results, two reactions should occur during sulfidation:

$$ZnO \text{ (s)} + H_2S \text{ (g)} \rightarrow ZnS \text{ (s)} + H_2O \text{ (g)} \tag{6}$$

$$ZnCO_3 \text{ (s)} + H_2S \text{ (g)} \rightarrow ZnS \text{ (s)} + CO_2 \text{ (g)} + H_2O \text{ (g)} \tag{7}$$

Nevertheless, we might also assume that reaction (Equation (7)) occurs in two steps, at first decomposition of $ZnCO_3$ by reaction (Equation (5)), pursued by reaction (Equation (6)):

$$1\text{st step } ZnCO_3 \text{ (s)} \rightarrow ZnO \text{ (s)} + CO_2 \text{ (g)}$$

$$2\text{nd step } ZnO \text{ (s)} + H_2S \text{ (g)} \rightarrow ZnS \text{ (s)} + H_2O \text{ (g)}$$

These various analyses have demonstrated several keys findings: firstly, that the A310 sorbent used in this study contained Zinc in two forms: ZnO and $ZnCO_3$. Despite this mixte composition, it proved to be an effective sorbent for capturing H_2S. Desulfurization is currently a significant challenge and discovering new sorbents for H_2S removal is crucial. The pursuit of pure metals oxide like ZnO is often time and cost- intensive. This study shows that the quest for such purity may not be necessary and a sorbent containing both ZnO and $ZnCO_3$ could be a viable alternative, playing an effective role in H_2S removal.

In order to determine the sulfidation mechanism in a sorbent containing both ZnO and $ZnCO_3$, a thermodynamic analysis is proposed in the following section.

3.3. Thermodynamics Calculations

The analyses of the Hi-Fuel sorbent used in our experimentations showed that the sorbent contained two chemical forms of zinc: ZnO and $ZnCO_3$. The part of $ZnCO_3$ estimated from the carbon concentration was 12.3 *w/w* % of fresh sorbent. Considering this composition, the thermodynamic calculations were carried out for two reactions: (6) and (7). All thermodynamical calculations were based on standard molar enthalpy of formation and standard molar entropy of pure substances at 298 K (25 °C) given in the study of Binnewies and Mike [40].

The enthalpy and entropy values for other temperatures were obtained by using the Equations (8) and (9):

$$\triangle_R H_T^0 = \triangle_R H_{298}^0 + \int_{298}^{T} C_p^0 dT \tag{8}$$

$$S_T^0 = S_{298}^0 + \int_{298}^{T} C_P^0 \frac{dT}{T} \tag{9}$$

with

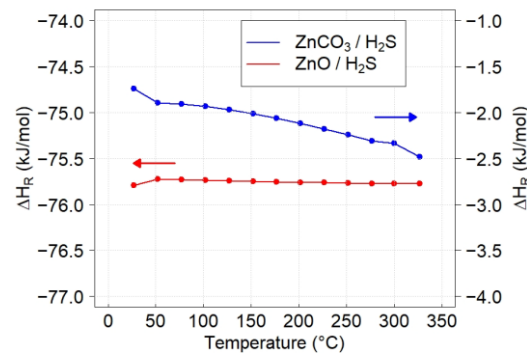$$C_P^0 = a + b \cdot 10^{-3} \cdot T + c \cdot 10^6 \cdot T^{-2} + d \cdot 10^{-6} \cdot T^2 \tag{10}$$

The coefficients a, b, c, d needed for each reagent in reactions (6) and (7) were given in thermochemical data [40].

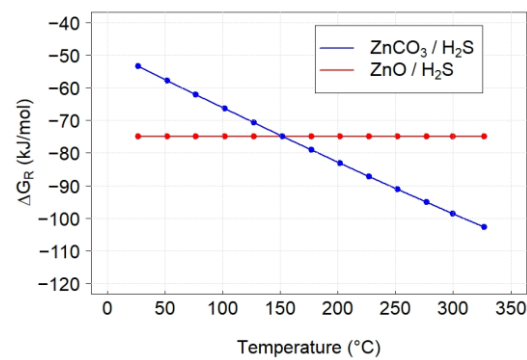After that, according to the Equations (11) and (12):

$$\Delta G_R(T) = \Delta H_R(T) - T\Delta S_R(T) \tag{11}$$
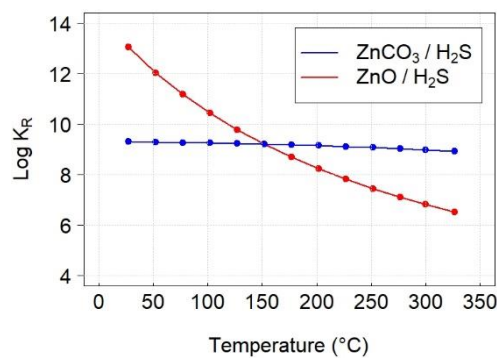
$$\ln K_R = -\frac{\Delta G_R}{RT} \tag{12}$$

We calculated the equilibria constants (K_R) for reactions (6) and (7). The results of these calculations are shown in Figures 10–12.

Figure 10. Enthalpy difference calculated for sulfidation reactions of ZnO and $ZnCO_3$.

Figure 11. Gibbs energy (ΔG_R) calculated for sulfidation reactions of ZnO and $ZnCO_3$.

Figure 12. Equilibrium constant (K_R) calculated for sulfidation reactions of ZnO and $ZnCO_3$.

The two reactions of H_2S with ZnO and $ZnCO_3$ are exothermic, and their enthalpies are relatively stable over the studied temperatures range (Figure 10). But the Gibbs energy (Figure 11) calculated for these reactions depicts a strong dependence of ΔG_R with temperature for the reaction of $ZnCO_3$ with H_2S. Below 152 °C, the sulfidation of ZnO seems favored, but above this temperature it seems that the reaction with $ZnCO_3$ would be preferential.

Based on ΔG_R for these two reactions, the equilibrium constants (K_R) show a similar evolution (Figure 12).

Two reactions occur in the studied temperatures range. But according to thermodynamical calculations, from 425 K (152 °C), the $ZnCO_3$ reaction with H_2S is privileged compared to the one between ZnO and H_2S (Figure 12).

At 300 °C, the process temperature in our test, the $ZnCO_3$ reaction with H_2S is highly favored (Table 3). As a comparison, other values from the literature for K_R of the reaction

ZnO + H₂S at 300 °C are 1.67×10^7 [41] or 3.58×10^7 as calculated from the equation in Samokhvalov et al. [36]. Both values lower to K_R of $ZnCO_3$ + H₂S confirm the reaction of $ZnCO_3$ with H₂S thermodynamically favored.

Table 3. Enthalpy (ΔH_R), entropy (ΔS_R), Gibbs energy (ΔG_R), and equilibrium constant (K_R) for the reactions at 300 °C of ZnO or $ZnCO_3$ with H₂S.

Reaction	ΔH_R (kJ/mol)	ΔS_R (J/mol·K)	ΔG_R (kJ/mol)	K_R
$ZnO + H_2S \rightarrow ZnS + H_2O$	−75.77	−1.6	−74.87	6.6×10^6
$ZnCO_3 + H_2S \rightarrow ZnS + CO_2 + H_2O$	−2.33	167.9	−98.54	9.5×10^8

Moreover, according to Balichard et al. [21], during the transformation of $ZnCO_3$-ZnS, the molar volume decreases (from 27.9 to 23.8 cm³/mol), contrary to the transformation of ZnO-ZnS, where the molar volume increases (from 14.5 to 23.8 cm³/mol). Therefore, the sorbent porosity is not reduced in the case of the first transformation. The exchange of gases in the sorbent pores is then facilitated.

4. Conclusions

We studied the sulfidation process of Hi-Fuel sorbent in a packed bed at 300 °C. The analyses carried out for this sorbent permitted us to conclude that the sorbent contained two types of zinc chemical compound: zinc oxide and zinc carbonate. The stability of the last compound depends on temperature. A thermal treatment of the packed bed for 6 h partially decompose the zinc carbonate (mass loss of sorbent = 1.2 *w/w* %) and the pore volume of mesopores increases. As the result, the H₂S access to the internal layers of sorbent particles must be enhanced and the sulfidation reaction can be facilitated. However, according to TGA, elemental, FTIR, and Raman analyses, this compound was still present in the sorbent after 22 days of experiment. The sulfidation of the tested sorbent, confirmed by many analyses, showed the gradient of conversion ratio (α) from the top (α = 0.27) to the bottom (α = 0.08) of the packed bed. Moreover, the thermodynamical calculations concluded that the reaction between zinc carbonate and hydrogen sulfide should be preferred. In summary, the Hi-Fuel A310 sorbent showed good efficiency for removing hydrogen sulfide from polluted gas. The height of the bed must be judiciously chosen when considering the conversion gradient of sorbent in the packed bed and to deeply (on the level of ppb) decontaminate the gas in industrial applications. With a focus on improvement, conducting comparative studies involving pure ZnO or pure $ZnCO_3$ would provide a more accurate determination of the kinetic differences among the various sorbents.

Author Contributions: Conceptualization, C.L., B.M., J.C. and P.P.; methodology, C.L., B.M. and J.C.; validation, P.P.; investigation, C.L., B.M., J.C., V.B. and N.R.; data curation, N.R., V.B. and B.M.; formal analysis, C.L., B.M., V.B. and N.R.; writing—original draft preparation, C.L.; writing—review and editing, B.M., J.C., N.R. and P.P.; visualization, J.C. and N.R.; supervision, P.P.; project administration, P.P.; funding acquisition, P.P. All authors have read and agreed to the published version of the manuscript.

Data Availability Statement: The original contributions presented in the study are included in the article, further inquiries can be directed to the corresponding author.

Conflicts of Interest: The authors declare no conflict of interest. The funders had no role in the design of the study; in the collection, analyses, or interpretation of data; in the writing of the manuscript; or in the decision to publish the results.

References

1. Frilund, C.; Kurkela, E.; Hiltunen, I. Development of a simplified gas ultracleaning process: Experiments in biomass residue-based fixed-bed gasification syngas. *Biomass Conv. Bioref.* **2021**, *13*, 15673–15684. [CrossRef]
2. Li, X.; O'Moore, L.; Song, Y.; Bond, P.L.; Yuan, Z.; Wilkie, S.; Hanzic, L.; Jiang, G. The rapid chemically induced corrosion of concrete sewers at high H2S concentration. *Water Res.* **2019**, *162*, 95–104. [CrossRef]
3. Legras, B.; Ordomsky, V.V.; Dujardin, C.; Virginie, M.; Khodakov, A.Y. Impact and Detailed Action of Sulfur in Syngas on Methane Synthesis on Ni/γ-Al$_2$O$_3$ Catalyst. *ACS Catal.* **2014**, *4*, 2785–2791. [CrossRef]
4. *ISO 14687:2019*; Hydrogen Fuel Quality—Product Specification. International Organization for Standarization: Geneva, Switzerland, 2019.
5. National Physical Laboratory (NPL). Available online: https://www.npl.co.uk/products-services/environmental/hydrogen-purity-for-fuel-cell-vehicles (accessed on 29 June 2021).
6. Huiling, F.; Yanxu, L.; Chunhu, L.; Hanxian, G.; Kechang, X. The apparent kinetics of H2S removal by zinc oxide in the presence of hydrogen. *Fuel* **2002**, *81*, 91–96. [CrossRef]
7. Skrzypski, J.; Bezverkhyy, I.; Heintz, O.; Bellat, J.P. Low Temperature H2S Removal with Metal-Doped Nanostructure ZnO Sorbents: Study of the Origin of Enhanced Reactivity in Cu-Containing Materials. *Ind. Eng. Chem. Res.* **2011**, *50*, 5714–5722. [CrossRef]
8. Neveux, L.; Chiche, D.; Bazer-Bachi, D.; Favergeon, L.; Pijolat, M. New insight on the ZnO sulfidation reaction: Evidences for an outward growth process of the ZnS phase. *Chem. Eng. J.* **2012**, *181–182*, 508–515. [CrossRef]
9. Yang, H.; Cahela, D.R.; Tatarchuk, B.J. A study of kinetic effects due to using microfibrous entrapped zinc oxide sorbents for hydrogen sulfide removal. *Chem. Eng. Sci.* **2008**, *63*, 2707–2716. [CrossRef]
10. Babé, C.; Tayakout-Fayolle, M.; Geantet, C.; Vrinat, M.; Bergeret, G.; Huard, T.; Bazer-Bachi, D. Crystallite size effect in the sulfidation of ZnO by H2S: Geometric and kinetic modelling of the transformation. *Chem. Eng. Sci.* **2012**, *82*, 73–83. [CrossRef]
11. Karmakar, M.K.; Chandra, P.; Chatterjee, P.K. A review on the fuel gas cleaning technologies in gasification process. *J. Environ. Chem. Eng.* **2015**, *3*, 689–702. [CrossRef]
12. Frilund, C.; Simell, P.; Kaisalo, N.; Kurkela, E.; Koskinen-Soivi, M.-L. Desulfurization of Biomass Syngas Using ZnO-Based Adsorbents: Long-Term Hydrogen Sulfide Breakthrough Experiments. *Energy Fuels* **2020**, *34*, 3316–3325. [CrossRef]
13. Westmoreland, P.R.; Gibson, J.B.; Harrison, D.P. Comparative kinetics of high-temperature reaction between hydrogen sulfide and selected metal oxides. *Environ. Sci. Technol.* **1977**, *11*, 488–491. [CrossRef]
14. Xue, M.; Chitrakar, R.; Sakane, K.; Ooi, K. Screening of adsorbents for removal of H2S at room temperature. *Green Chem.* **2003**, *5*, 529–534. [CrossRef]
15. Sohn, H.Y.; Szekely, J.A. Structural model for gas-solid reactions with a moving boundary—III. *Chem. Eng. Sci.* **1972**, *27*, 763–778. [CrossRef]
16. Sadegh-Vaziri, R.; Babler, M.U. Numerical investigation of the outward growth of ZnS in the removal of H2S in a packed bed of ZnO. *Chem. Eng. Sci.* **2017**, *158*, 328–339. [CrossRef]
17. Bezverkhyy, I.; Skrzypski, J.; Safonova, O.; Bellat, J.P. Sulfidation Mechanism of Pure and Cu-Doped ZnO Nanoparticles at Moderate Temperature: TEM and In Situ XRD Studies. *J. Phys. Chem. C* **2012**, *116*, 14423–14430. [CrossRef]
18. Liu, Y.; Zhao, J.; Zhang, H.; Zhu, Y.; Wang, Z. Thermal decomposition of basic zinc carbonate in nitrogen atmosphere. *Thermochim. Acta* **2004**, *414*, 121–123. [CrossRef]
19. Hales, M.C.; Frost, R.L. Thermal analysis of smithsonite and hydrozincite. *J. Therm. Anal. Calorim.* **2008**, *91*, 855–860. [CrossRef]
20. Kowalik, P.; Konkol, M.; Antoniak-Jurak, K.; Próchniak, W.; Wiercioch, P.; Rawski, M.; Borowiecki, T. Structure and morphology transformation of ZnO by carbonation and thermal treatment. *Mater. Res. Bull.* **2015**, *65*, 149–156. [CrossRef]
21. Balichard, K.; Nyikeine, C.; Bezverkhyy, I. Nanocrystalline ZnCO$_3$—A novel sorbent for low-temperature removal of H2S. *J. Hazard. Mater.* **2014**, *264*, 79–83. [CrossRef]
22. Brunauer, S.; Emmett, P.H.; Teller, E. Adsorption of Gases in Multimolecular Layers. *J. Am. Chem. Soc.* **1938**, *60*, 309–319. [CrossRef]
23. Holbrook, R.D.; Galyean, A.A.; Gorham, J.M.; Herzing, A.; Pettibone, J. Overview of Nanomaterial Characterization and Metrology. *Front. Nanosci.* **2015**, *8*, 47–87. [CrossRef]
24. Palchoudhury, S.; Baalousha, M.; Lead, J.R. Methods for Measuring Concentration (Mass, Surface Area and Number) of Nanomaterials. *Front. Nanosci.* **2015**, *8*, 153–181. [CrossRef]
25. Florén, C.R. Development of Desulphurisation Unit for Fuel Cell System. Master's Thesis, Chalmers University of Technology, Göteborg, Sweden, 2015; p. 88.
26. Kanari, N.; Mishra, D.; Gaballah, I.; Dupré, B. Thermal decomposition of zinc carbonate hydroxide. *Thermochim. Acta* **2004**, *410*, 93–100. [CrossRef]
27. Castellano, M.; Matijevic, E. Uniform colloidal zinc compounds of various morphologies. *Chem. Mater.* **1989**, *1*, 78–82. [CrossRef]

28. Sharma, D.; Jha, R. Analysis of structural, optical and magnetic properties of Fe/Co co-doped ZnO nanocrystals. *Ceram. Int.* **2017**, *43*, 8488–8496. [CrossRef]

29. Winiarski, J.; Tylus, W.; Winiarska, K.; Szczygieł, I.; Szczygieł, B. XPS and FT-IR Characterization of Selected Synthetic Corrosion Products of Zinc Expected in Neutral Environment Containing Chloride Ions. *J. Spectrosc.* **2018**, *2018*, 1–14. [CrossRef]

30. Vágvölgyi, V.; Hales, M.; Martens, W.; Kristóf, J.; Horváth, E.; Frost, R.L. Dynamic and controlled rate thermal analysis of hydrozincite and smithsonite. *J. Therm. Anal. Calorim.* **2008**, *92*, 911–916. [CrossRef]

31. Koga, N.; Goshi, Y.; Yamada, S.; Pérez-Maqueda, L.A. Kinetic approach to partially overlapped thermal decomposition processes: Co-precipitated zinc carbonates. *J. Therm. Anal. Calorim.* **2013**, *111*, 1463–1474. [CrossRef]

32. Milekhin, A.G.; Yeryukov, N.A.; Sveshnikova, L.L.; Duda, T.A.; Himcinschi, C.; Zenkevich, E.I.; Zahn, D.R.T. Resonant Raman scattering of ZnS, ZnO, and ZnS/ZnO core/shell quantum dots. *Appl. Phys. A* **2012**, *107*, 275–278. [CrossRef]

33. Fairbrother, A.; Izquierdo-Roca, V.; Fontané, X.; Ibáñez, M.; Cabot, A.; Saucedo, E.; Pérez-Rodríguez, A. ZnS grain size effects on near-resonant Raman scattering: Optical non-destructive grain size estimation. *CrystEngComm* **2014**, *16*, 4120–4125. [CrossRef]

34. Kim, J.H.; Rho, H.; Kim, J.; Choi, Y.J.; Park, J.G. Raman spectroscopy of ZnS nanostructures: Raman spectroscopy of ZnS nanostructures. *J. Raman Spectrosc.* **2012**, *43*, 906–910. [CrossRef]

35. Scott, S.D.; Barnes, H.L. Sphalerite-wurtzite equilibria and stoichiometry. *Geochim. Cosmochim. Acta* **1972**, *36*, 1275–1295. [CrossRef]

36. Samokhvalov, A.; Tatarchuk, B.J. Characterization of active sites, determination of mechanisms of H_2S, COS and CS_2 sorption and regeneration of ZnO low-temperature sorbents: Past, current and perspectives. *Phys. Chem. Chem. Phys.* **2010**, *13*, 3197–32092011. [CrossRef] [PubMed]

37. Li, L.; King, D.L. H_2S removal with ZnO during fuel processing for PEM fuel cell applications. *Catal. Today* **2006**, *116*, 537–541. [CrossRef]

38. Gültekin, D.; Akbulut, H. Raman Studies of ZnO Products Synthesized by Solution Based Methods. *Acta Phys. Pol. A* **2016**, *129*, 803–805. [CrossRef]

39. RRUFF Project. ID: 040035. Available online: https://rruff.info/R040035 (accessed on 1 February 2021).

40. Binnewies, M.; Milke, E. *Thermochemical Data of Elements and Compounds*, 2nd ed.; Wiley-VCH Verlag GmbH: Weinheim, Germany, 2002. [CrossRef]

41. Neveux, L. Study of the kinetics and mechanism of ZnO sulfidation by H2S. Ph.D. Thesis, Ecole Nationale Supérieure des Mines de Saint Etienne, Saint Etienne, France, 2011; p. 31.